Korean J. Chem. Eng., 33(6), 1767-1776 (2016)
DOI: 10.1007/s11814-016-0074-x
pISSN: 0256-1115
eISSN: 1975-7220

REVIEW PAPER

Dynamic modeling and simulation of reaction, slag behavior, and heat transfer to water-cooling wall of shell entrained-flow gasifier

Cheol-Oong Kim*,‡, Ryang-Gyoon Kim,‡, Zelin Wu***, and Chung-Hwan Jeon***,†**

*Senior Researcher, Energy Technology Team, GS Engineering & Construction Co., Ltd., Seoul 03159, Korea
**Senior Researcher, PosCC (Clean Coal), Research Institute of Industrial Science & Technology, Pohang 37673, Korea
***School of Mechanical Engineering, Pusan Clean Coal Center, Pusan National University, Busan 46241, Korea
(*Received 9 August 2015 • accepted 6 March 2016*)

Abstract−A mathematical model is developed to simulate a pilot Shell entrained-flow coal gasifier. Submodels of specific structures of the gasifier are established to simulate the complicated gasification process. The model includes the total energy conservation equation and mass conservation equations for the gas components, solid flow, and gas flow. It simulates the influence of the gasifier structure and dimensions and can calculate the effects of changing almost every important operation parameter, e.g., the syngas composition, gasification temperature, carbon conversion ratio, wall-layer temperature, and slag mass flow rate. The model can predict the syngas composition under a limited residence time condition. Furthermore, it considers the heat transfer coefficient of each layer of the water wall to calculate its heat loss and temperature. Thus, the model also reflects the influence of performance parameters of the gasifier's water wall. The slag mass flow rate on the wall is calculated using a slag submodel.

Keywords: Entrained-flow Gasifier, Dynamic Modelling, Simulation, Reaction, Water Wall Heat Transfer, Slag Behavior

INTRODUCTION

One commercial plant project in South Korea employs the coal gasification technology. A 300-MW-class Integrated Gasification Combined Cycle (IGCC) plant based on the Shell gasifier is being constructed by Korea Western Power, a power plant company. In parallel, various design technology developments of a gasification block of the plant, such as reviewing the effect of operation factors on the gasifier, have also been progressing [1]. The IGCC is a coal gasification technology, coal gas purification technology, and high-performance combined gas turbine and steam turbine cycle technology; it further involves the process integration. The IGCC also differs from the conventional gas-steam combined cycle mainly in terms of the coal gasification and purification systems and equipment [2-5]. Therefore, research aimed at the development of large-capacity and high-energy-conversion-efficiency coal gasifiers is the key to achieving an IGCC power generation scheme.

Several models for studying the gasification process in the gasifier have been established [6-8]; in particular, entrained-flow gasifiers have been the object of extensive research. Some early research considered a stable state in the gasification process in order to analyze the influence of different operating conditions on the gasifier performance. For instance, Wen developed a mathematical model for simulating the Texaco pilot-plant down-flow entrained gasifier [6]. Govind simulated the Texaco pilot-plant down-flow gasifier by simultaneously solving the mass, momentum, and energy balance equations for the solid and gas phases [9]. Matteo conducted simulation studies using the Aspen Plus software for the Shell gasifier IGCC system to determine the water-wall temperature, the composition and temperature of the gasifier outlet gas, and a rule for determining changes in the gasifier performance so as to build a foundation for further research on IGCC performance [10]. Sun developed a dynamic model of the Shell gasifier IGCC system on the basis of physical principles, by focusing on the time-dependent accumulation and flow on the walls [11,12]. These studies on the performance of entrained-flow gasifiers have provided crucial knowledge on the gasification process.

At present, two types of methods are available for modeling the gasification process in the gasifier. One is thermodynamic modeling. In this modeling, according to the laws of thermodynamics, the mass balance equation for different materials and the energy balance equation are formulated, and then, the equilibrium gasification temperature and gas composition are estimated under given operating conditions. This permits estimation of the influence of the gasifier size on the gasification process. The other type of method is dynamic modeling in which the dynamics of the main chemical reactions in the gasifier are considered along with the gasifier structure and operating conditions. Then, the gas component temperature and coal conversion ratio are forecast, and finally, the gasifier performance is evaluated accordingly. In the present work, a dynamic model of the gasification performance of the Shell coal gasifier is proposed.

The proposed mathematical model considers in detail the gas and solid flow processes as well as the combustion reaction and the dynamic water-gas reaction process. The model not only estimates the influence of the gasifier structure size but also calculates the main gasifier performance parameters. The structure of the Shell

†To whom correspondence should be addressed.
E-mail: chjeon@pusan.ac.kr
‡These authors contributed equally to this work.

gasifier includes a number of water tubes around the gasifier itself. Therefore, the proposed model considers the temperature difference between the inside and outside of the gasifier and uses the heat transfer coefficient of each layer of the gasifier wall to calculate its heat loss and temperature, and to thus determine the influence of the water-wall performance parameters. A layer of refractory material is applied to the inside of the wall, where high-temperature molten slag flows and where it can ultimately cool and solidify to stick to the wall. The resulting mixed slag layer is considered normal during operation of the gasifier. Therefore, this study also focuses on the mass flow rate of the slag layer.

GASIFICATION PROCESS

Gasification processes are classified according to the method used to bring the coal into contact with the gasifying medium (air or oxygen). The three main commercial modes are the fixed-bed, fluidized-bed, and entrained-flow-bed modes. This study focuses on an entrained-flow gasifier. In an entrained-flow reactor, small condensed particles (in the solid or slurry state) are dispersed and entrained in a moving gaseous medium. This provides a larger surface contact area for a reaction, and it can induce a reduction in the gas-solid diffusion resistance to enable a rapid chemical reaction between the solid and gas phases. Furthermore, the particles can be entrained in the gasifying medium itself to react in a co-current flow in a high-temperature flame. The residence time in this type of gasifier is extremely short. Entrained-flow gasifiers generally use oxygen as the oxidant and operate at high temperatures, which are well above ash-slagging conditions, to ensure high carbon conversion ratio.

MODELING ASSUMPTIONS

A one-dimensional model of the reactor system is constructed. The following are the basic assumptions made for constructing the model.

(1) The solid and gas phases are assumed to be completely mixed. The nature of mixing between these phases can have a significant effect on the final carbon conversion ratio and product composition.

(2) The system is assumed to be highly dilute, and so, interactions among particles can be neglected. A slag layer is assumed to remain on the particle surface.

(3) The ideal gas equation of state is assumed to hold.

(4) The temperature is assumed to be uniform throughout the solid particles.

(5) Ash is assumed to be inert and to remain with the particles. The effect of ash as a catalyst is formally neglected, although this effect may have been accounted for indirectly during the establishment of the kinetic equations.

(6) Particle attrition is considered not to occur.

(7) Because of the high temperature in the reactor, the potential and kinetic energies are neglected in comparison to the thermal energy.

(8) The slag layer is in the liquid state.

EQUATIONS

In the proposed model, the mass, energy, and momentum conservation equations are considered to vary only along the axis of division within the reactor, and the gas and solid phases are treated as pseudo-fluids. The conservation equations presented in Table 1 are

Table 1. Conservation equations

Conservation	Equation	Variable
Gas-phase species	$\frac{\partial(C_i\varepsilon_g)}{\partial t}=-u_g\frac{\partial(C_i\varepsilon_g)}{\partial x}+\varepsilon_g D_g\frac{\partial^2 C_i}{\partial x^2}+R_{hom,\,i}+R_{dev,\,i}/mw_i$	C_i gas-phase concentration
Solid-phase species mass	$\frac{\partial(A_{cs}\rho_{coal\text{-}af}\varepsilon_s)}{\partial t}=-\frac{\partial(A_{cs}\rho_{coal\text{-}af}\varepsilon_s u_s)}{\partial x}-A_{cs}\varepsilon_s(R_{het}+R_{dev,\,tot})$	$\rho_{coal\text{-}af}$ density of ash-free coal
Gas-phase energy	$\frac{\partial(A_{cs}\varepsilon_g\rho_g Cp_g T_g)}{\partial t}=-\frac{\partial(A_{cs}\varepsilon_g\rho_g h_g u_g)}{\partial x}+A_{cs}k_g\frac{\partial^2 T_g}{\partial x^2}$ $+A_{cs}\left(\varepsilon_g\sum_{hom}h_{hom}R_{hom}mw_i-\varepsilon_s\sum_{het}h_{het}R_{het}\right)+A_{cs}h_iR_{dev,\,i}$ $-Q_{conv,\,g\to p}-Q_{rad,\,p\to g}-Q_{conv,\,g\to wall}$	T_g gas-phase temperature
Solid-phase energy	$\frac{\partial(A_{cs}\varepsilon_s\rho_s Cp_s T_s)}{\partial t}=\frac{\partial(A_{cs}\varepsilon_s\rho_s h_s u_s)}{\partial x}-A_{cs}\sum_{het}h_{het}R_{het}-A_{cs}h_iR_{dev,\,i}$ $+Q_{conv,\,s\to g}+Q_{rad,\,s\to g}-Q_{rad,\,s\to wall}-+Q_{conv,\,s\to wall}$	T_s solid-phase temperature
Gas-phase momentum	$\frac{\partial(A_{cs}\varepsilon_g\rho_g u_g)}{\partial t}=-\frac{\partial(A_{cs}\varepsilon_g\rho_g u_g^2)}{\partial x}+A_{cs}\left(\rho_g g\varepsilon_g-F_{g-w}-F_{g-s}-\frac{\partial P}{\partial x}\right)$	u_g gas-phase velocity
Solid-phase momentum	$\frac{\partial(A_{cs}\varepsilon_s\rho_s u_s)}{\partial t}=-\frac{\partial(A_{cs}\varepsilon_s\rho_s u_s^2)}{\partial x}+A_{cs}(\rho_s g\varepsilon_s+F_{g-s})$	u_s solid-phase velocity
Slag mass flow	$m_{slag.lim}=\frac{u_s}{d}\frac{4\pi r_p^3}{3}\rho_{slag}\frac{2\pi r_{gasifier}}{r_p}$	m_{slag} slag mass flow
Membrane wall energy	$\frac{\partial(A_{cs,\,l}\rho_l Cp_l T_l)}{\partial t}=A_{cs,\,l}k_l\frac{\partial^2 T_l}{\partial x^2}+Q_{cond-l}+Q_{cond+l}$	T_l wall-layer temperature

Table 2. Rate expressions of homogeneous reactions

Reaction	Rate expression
$CO+\frac{1}{2}O_2 \xrightarrow{k_1} CO_2$	$R_1=10^5[CO][O_2]^{0.25}[H_2O]^{0.5}$
$H_2+\frac{1}{2}O_2 \underset{-k_1}{\overset{+k_1}{\rightleftharpoons}} H_2O$	$R_2=10^8([H_2]^{0.25}[O_2]^{1.5}-[H_2O]/K_1)$
$CH_4+\frac{1}{2}O_2 \xrightarrow{k_3} CO+2H_2$	$R_3=10^8[CH_4][O_2]^{1.25}$
$CO+H_2O \underset{-k_4}{\overset{+k_4}{\rightleftharpoons}} CO_2+H_2$	$R_4=2.75\times10^9\exp(-10072/T_g)\times([CO][H_2O]-[CO_2][H_2]/K_4)$
$CH_4+H_2O \xrightarrow{k_5} CO+3H_2$	$R_5=10^5[CH_4][H_2O]$
$C_2H_6+O_2 \xrightarrow{k_6} 2CO+3H_2$	$R_6=10^8[C_2H_6][O_2]^{1.25}$
$Tar+O_2 \xrightarrow{k_7} CO+H_2+SO_2+N_2$	$R_7=10^8[Tar][O_2]^{1.25}$

one-dimensional in the axial direction; they are treated as dynamic equations in the model, even for steady-state simulations.

SUBMODELS

1. Devolatilization

In the gasifier, the temperature is typically higher than 1,300 K. Therefore, devolatilization occurs because of a rapid temperature increase, and moisture evaporates completely when material enters the reactor. When coal is fed into the gasifier, it first undergoes pyrolysis and decomposes into volatile matter and char, as expressed by Eq. (1):

$$C_aH_bO_cN_dS_e \xrightarrow{dev} \partial CO+\beta CO_2+\chi H_2+\delta H_2O+\varepsilon CH_4 +\phi C_2H_6+\gamma NH_3+\eta H_2S+\lambda tar+\varphi char \quad (1)$$

The volatile composition and yield are modeled using the Merrick model [12]. The final limitation on devolatilization is the relation between the actual volatile yield and the initial volatile matter (vm) content obtained by proximate analysis:

$$Y_{vm}=X_{vm,0}-0.36X_{vm,0}^2 \quad (2)$$

Devolatilization of gas-phase species is expressed as

$$R_{dev,i}=\varepsilon_p X_{daf} X_{dev,i}\rho_s/t_{dev} \quad (3)$$

The total volatile matter is given as

$$R_{dev,tot}=-\sum_i R_{dev,i} \quad (4)$$

2. Homogeneous Reactions

Rate expressions of homogeneous reactions are of the form $R_{het}=k_{het}[\chi_a]^a[\chi_b]^b$, and the unit for the rate is kmol/m^3/s. The homogeneous reaction rate expressions considered in the proposed model are presented in Table 2. The global kinetics of the homogeneous reactions for major species are modeled using the rate expressions derived by Jones and Lindstedt [13] and Westbrook and Dryer [14]. The equilibrium coefficients for homogeneous reactions are taken from the NIST-JANAF Thermochemical Tables [15]. For an irreversible homogeneous reaction, the value of k_{het} is calculated over the expected temperature range inside the gasifier.

3. Heterogeneous Reactions

The model considers four heterogeneous reactions as expressed below:

$$C_\alpha H_\beta O_\chi N_\varepsilon S+\left(\frac{\alpha}{\phi}+\frac{\beta}{4}-\frac{\chi}{2}-\frac{3\delta}{4}\right)O_2 \rightarrow 2\alpha\left(1-\frac{1}{\phi}\right)CO +\alpha\left(\frac{2}{\phi}-1\right)CO_2+\left(\frac{\beta-3\delta-2\varepsilon}{2}\right)H_2O+\delta NH_3+\varepsilon H_2S \quad (5)$$

$$C_\alpha H_\beta O_\chi N_\varepsilon S+(\alpha-\beta)H_2O \rightarrow \alpha CO+\alpha\left(\frac{2}{\phi}-1\right)CO_2 +\left(\frac{2\alpha+\beta-2\chi-3\delta-2\varepsilon}{2}\right)H_2+\delta NH_3+\varepsilon H_2S \quad (6)$$

$$C_\alpha H_\beta O_\chi N_\varepsilon S+\alpha CO_2 \rightarrow 2\alpha CO+\left(\frac{\beta-2\chi-3\delta-2\varepsilon}{2}\right)H_2+\delta NH_3+\varepsilon H_2S \quad (7)$$

$$C_\alpha H_\beta O_\chi N_\varepsilon S+\left(\frac{4\alpha-\beta+2\chi+3\delta+2\varepsilon}{2}\right)H_2 \rightarrow \chi H_2O+\alpha CH_4+\delta NH_3+\varepsilon H_2S \quad (8)$$

For the char oxidation reaction, a mechanism factor ϕ is used to account for direct conversion of carbon to carbon dioxide at low temperatures [16]. This factor is estimated according to the method described in Table 3.

Heterogeneous reaction kinetics is modeled using *n*-order rate expressions. Kinetic data can be input into the model in the form of intrinsic variables. These intrinsic kinetic data are used to calculate an intrinsic reaction rate constant for the heterogeneous reaction. The heterogeneous rate parameters for coal are listed in Table 4. When the intrinsic kinetic data are used, the partial pressure of each reactant at the particle surface is determined by calculating its rate of diffusion through a boundary layer around the particle. The

Table 3. Mechanism factor

Dp (cm)	ϕ	Comment
<0.005	$\frac{2Z+2}{Z+2}$	
0.005-0.1	$\frac{(2Z+2)-\frac{Z(d_p-0.005)}{0.095}}{Z+2}$	$Z=\frac{[CO]}{[CO_2]}=2500e^{-\frac{6249}{T}}$
>0.1	1.0	

Table 4. Kinetic rate parameters for CSIRO gasifier test coals from Ref. [28]

Reaction	Parameter	Unit	CRC358	CRC274	CRC299
$C+O_2$	A_{int}	$kg/m^2/s/atm^n$	319	13.8	601
	E_{int}	GJ/kmol	0.1605	0.138	0.1565
	η_{int}		0.8	0.8	0.8
$C+H_2O$	A_{int}	$kg/m^2/s/atm^n$	226	600	10400
	E_{int}	GJ/kmol	0.2382	0.228	0.2679
	η_{int}		0.4	0.4	0.4
$C+CO_2$	A_{int}	$kg/m^2/s/atm^n$	220	20000	83200
	E_{int}	GJ/kmol	0.2432	0.289	0.2905
	η_{int}		0.4	0.4	0.3

rate of this reaction (Eq. (9)) is expressed as

$$R_{het}=\left(1+\frac{6}{\eta_{int}d_p\rho_p S_{in}}\right)\eta_{int}S_{in}A_{int}\exp(-E_{int}/R_uT_p)(\eta_{ex}P_\infty)^n\rho_p \quad (9)$$

4. Slag Behavior

Sometimes mineral matter in coal can cause slagging problems during coal combustion, such as when Moolarben coal used in five coal-fired power plants in Korea was blended with low-quality coals and used in boilers [17]. Besides, it is more important to predict slag behavior in such as the Shell entrained-flow gasifier in order to get suitable operation conditions. The char particles may be trapped in the slag layer if impinging particles plunge deep into the layer. For this plunging to occur, the particle inertia needs to overcome viscous and interfacial forces, both of which counteract the penetration of the impinging particles into the wall slag layer. The driving force on a particle is associated with the normal component of the impact velocity of the char particle balanced against the slag viscous forces [18]. If the particles are trapped, the slag mass flow rate is affected by their capture efficiency and reaction rate [19,20]. If, however, they are not trapped, the slag mass flow rate is equal to the minimum flow rate. The slag viscosity is the criterion for judging whether or not particles are trapped.

$$\text{if: } r_pu_s>18\frac{\mu}{\rho_s}$$

$$\text{then: } -\frac{1}{A_{cs}}\frac{\partial m_{slag}}{\partial z}=-k_m\frac{u_{slag}}{2r_{solid}}\frac{4\pi r_p^3}{3}\rho_s\frac{2\pi r_{gasifier}}{r_pu_g}+\frac{A_{eff}}{A_{solid}}R_{het} \quad (10)$$

$$\text{else: } m_{slag.lim}=\frac{u_s}{d}\frac{4\pi r_p^3}{3}\rho_s\frac{2\pi r_{gasifier}}{r_p}$$

The slag viscosity is evaluated as a function of the slag composition and temperature by using the Urbain model [20]:

$$\mu_{slag}=aT\exp(10^3/T)$$

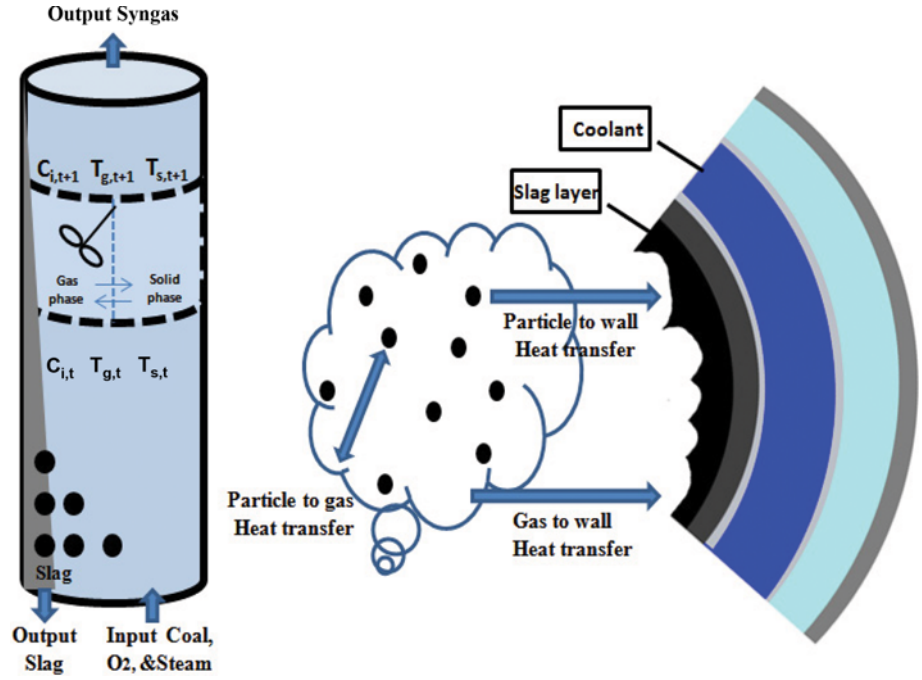

Fig. 1. Gasification process and evaluated heat transfer terms.

where (11)
$-\ln a=0.2693b+13.9751$

5. Heat Transfer

To obtain the heat flux and the temperature profile, the energy balance equation for each layer of the wall is written, as shown in Fig. 1. Both the heat transfer from the gas to the particles and that from the gas to the wall are considered along with the heat transfer from the external wall to the atmosphere. The Nusselt numbers for the gas-to-particle and gas-to-wall convections are calculated using the Petukhov equation [21]:

$$Nu_s=1.32Re_p^{0.5}Pr^{1/3} \tag{12}$$

$$Nu_w=(f/8)Re_wPr/(1.07+12.7(f/8)^{0.5}(Pr^{2/3}-1)) \tag{13}$$

The Nusselt number for external convection is calculated using the Churchill-Chu equation [22]:

$$Nu_{ext}=(0.825+0.387Ra_{ext}^{0.167})^2/[1+(0.492/Pr)^{0.5625}]^{0.5923} \tag{14}$$

The radiative heat transfer between particles is modeled using the radiation-as-diffusion (RAD) model [23]:

$$Q_{rad}=-\frac{64\delta T_s^3 r_{gasifier}^2}{3K}\frac{\partial T_s}{\partial x} \tag{15}$$

The Shell gasifier is equipped with a water-cooled membrane wall, where intermediate-pressure (IP) steam is produced inside high-pressure steel tubes present all around the reactor jacket. During operation, the solidified ash layer coating the wall acts as the primary thermal barrier [24]. A thin layer of refractory material—generally silicon carbide—is anchored to the tube surface between the steel and the solidified ash to prevent local damage and corrosion of the membrane wall [25]. Since the membrane wall cannot withstand a large pressure difference, vessel pressurization is maintained by means of an outer steel vessel, and an air layer is incorporated between the outer wall of the gasifier and the membrane wall [26]. As shown in Fig. 2, the composite wall can be divided into six layers: Slag and solid ash layer, silicon carbide (refractory) layer, tube jacket, steam/water mixture, air layer, and steel vessel and ambient air layer. The expressions of the heat transfer terms for these six layers for use in the energy conservation equations are as given below.

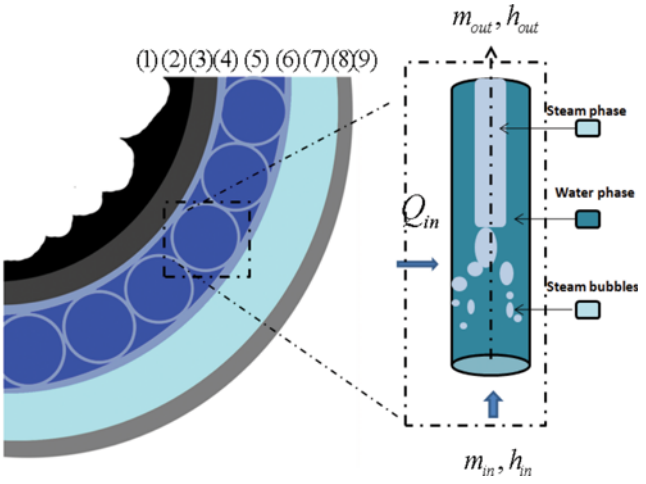

Fig. 2. Gasifier wall structure and cooling mechanism.

(1) Gas
(2) Slag
(3) Refractory
(4) $Membrane_{in}$
(5) Water
(6) $Membrane_{out}$
(7) Air
(8) Steel
(9) Ambient

$$Q_{cond,\,l}=2\pi k_l\frac{(T_l-T_{l+1})}{\ln(r_{l+1}/r_l)} \tag{16}$$

At the coolant tubes, heat is conducted across the tube walls into the water flowing upward through the tube, which induces a phase change. Determination of the heat transfer coefficient requires a complex calculation that takes into account the steam-liquid conditions at each location in the gasifier. The energy terms obtained by consideration of a control volume for the determination of the steam-water fraction are the convective heat flow from the tube and the enthalpy of the incoming/exiting water mixture [27]. The expressions for the coolant tubes are as follows:

$$m_{coolant\text{-}in}h_{coolant\text{-}out}+Q_{in}=m_{coolant\text{-}out}h_{coolant\text{-}out}$$
where
$$m_{coolant\text{-}in}=m_{coolant\text{-}out} \tag{17}$$
$$h_{coolant\text{-}out}=h_l(1-X)+Xh_g$$
$$Q_{in}=\frac{h_{mix}}{A_{contact}}\Delta T$$

The heat transfer coefficient of the mixture is expressed as

$$\frac{h_{mix}}{h_{sp}}=1.136\left(\frac{\rho_l}{\rho_v}\right)^{0.45}X^{0.72}(1-X)^{0.08}f(Fr) + 667.2\left(\frac{q_s''}{mh_{fg}}\right)^{0.7}(1-X)^{0.8}G_{sf} \tag{18}$$

SIMULATION AND METHODOLOGY

The modeling study was conducted using the general PROcess Modeling System (gPROMS). In gPROMS, the governing equation, boundary conditions, and initial conditions are necessary for the simulation. Three types of Australian bituminous coals were used in these simulations: CRC358 coal, CRC274 coal, and CRC299 coal. The gasifier operating conditions and coal compositions are presented in Table 5, and the schematic diagram of the Shell gasifier is shown in Fig. 11.

RESULTS AND DISCUSSION

1. Syngas Composition

To demonstrate the validity of the proposed entrained-flow gasifier model, the performance of the Shell gasifier was simulated. Data reported by Shell were used as reference data in the simulation [24]. The simulation results shown in Fig. 3 are close to the reference data. In particular, the exit gas compositions are roughly the same. The simulated carbon monoxide content is slightly higher than the reference value, because the conditions used for the model are slightly different from the actual operating conditions. At the exit, the simulated carbon dioxide content is slightly lower than the reference value.

Table 5. Gasifier operating conditions and coal compositions

	Dimensions of gasifier and membrane wall			
	Height	10 m	Tube diameter	0.2 m
	Inner diameter	3 m	Tube thickness	0.006 m
	Steel vessel thickness	0.06 m	Membrane pressure	54 atm
	Tube length	10 m	Refractory thickness	0.06
	Input date			
	Pressure	44 atm	Coal flow rate	49 kg/s
	Water pressure	54 atm	Air layer	0.6 m
	Particle diameter	100 μm	Gas inlet temperature	1373 K
	Oxygen/coal ratio	0.86	Steam/coal ratio	0.038
	Coal type	CRC358	CRC274	CRC299
	Proximate analysis			
	Fixed carbon	59.4%	58%	39.7%
	Volatile matter	19.2%	28%	24.3%
	Ash	20.2%	9.3%	25%
	Moisture	1.2%	4.7%	10.9%
	Ultimate analysis			
	C	69.6	72	52.1
	H	3.7	4.1	2.8
	O	3.3	7.8	8.1
	N	1.4	1.7	0.8
	S	0.7	0.4	0.3
	Ash	20.2	9.3	25
	Moisture	1.2	4.7	10.9

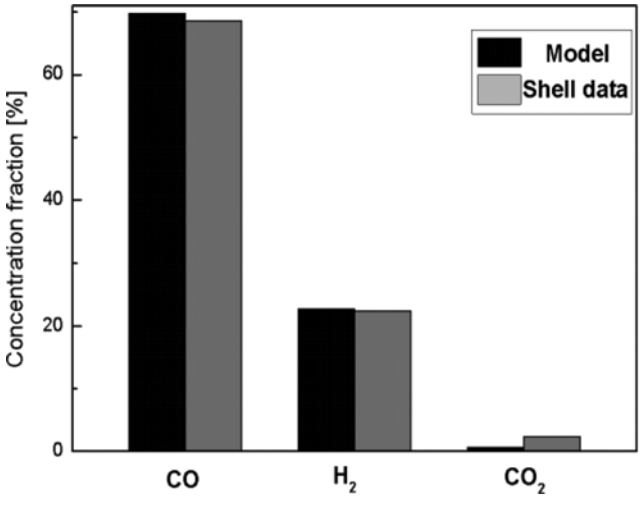

Fig. 3. Comparison of gas concentrations at gasifier outlet.

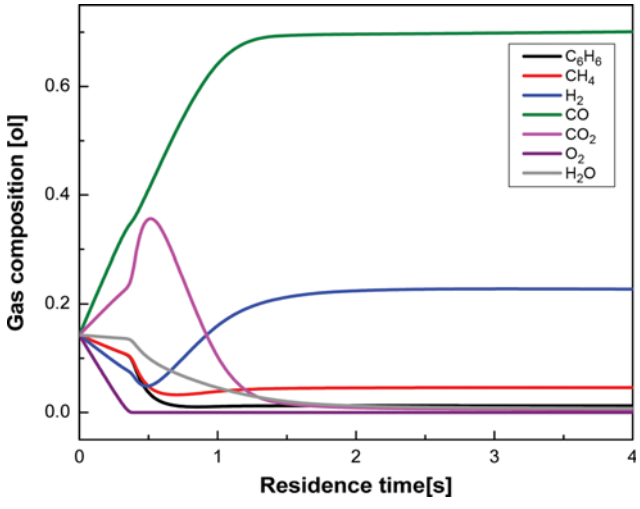

Fig. 4. Gas composition inside the gasifier at various times.

The gas composition inside the gasifier is shown in Fig. 4. The horizontal axis represents the residence time of the coal particles in the gasifier. According to the conservation of momentum, the coal particles are estimated to remain in the gasifier for at least 4s. Although the particle trajectory is uncertain, for simulating the gas composition dynamics, the model uses the minimum line distance to calculate the residence time of the coal particles. When these particles enter the gasifier, the oxygen concentration drops rapidly because of the subsequent combustion of the volatiles. This process also reduces the hydrogen concentration rapidly, but it increases the carbon dioxide concentration. Then, the carbon dioxide concentration reduces gradually; this reduction is an indicator of the end of the devolatilization and combustion processes and the beginning of the main gasification stage. In the main gasification stage, the carbon monoxide and hydrogen concentrations increase gradually. Under the input conditions considered here, this increase

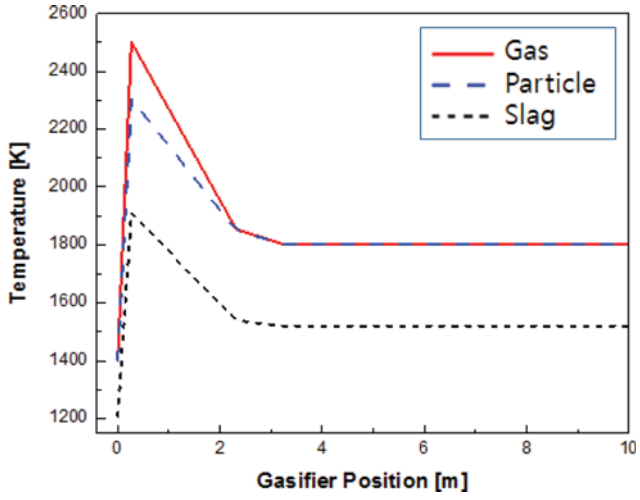

Fig. 5. Temperature profiles within axial component of gasifier.

leads to the production of a syngas consisting mainly of carbon monoxide. The amount of steam, which is the gasification agent, also reduces gradually in the main gasification stage. In the early stages, the steam concentration does not decrease rapidly. This is because the moisture in the coal is first removed in the high-temperature devolatilization process and is then consumed in the main gasification stage. Later on in the gasification stage, the gas composition becomes more stable.

2. Three Different Temperatures

The temperatures of the particles and gas together define the internal temperature of the gasifier. The temperature profiles of the different components inside the gasifier are shown in Fig. 5. At the entrance of the gasifier, the particle and gas temperatures increase rapidly because of rapid burning of the volatile components under the high concentration of oxygen. The particle and gas temperatures are obviously different at this location. Analysis of the reaction rates suggests that the gas combusts more rapidly and fully than the particles do. Further along the gasifier, the particle and gas temperatures decrease and eventually remain roughly the same. The computed temperature at the exit is 1,800 K, which is consistent with the temperature range provided by Shell. The slag temperature at the wall is also shown. The slag temperature is obviously lower than the temperature inside the gasifier, because of the heat transfer capability of the slag. Nevertheless, the slag temperature is still inevitably influenced by the internal temperature of the gasifier, and it increases and decreases accordingly.

Fig. 6 shows the temperature profile along the gasifier wall. From the slag layer to the water wall, the temperature reduces significantly, and beyond the water wall, it reduces more gradually. This trend meets the design requirements, depending on the temperature difference, while slagging occurs on the refractory layer. Because of the mass flow of water, the internal temperature of the water wall is radially uniform. The temperature of the outer wall of the gasifier is around 320-340 K, because the thick layer of air permits only weak radiative heat transfer.

3. Slag Viscosity and Mass Flow Rate

The slag viscosity and mass flow rate profiles are shown in Fig.

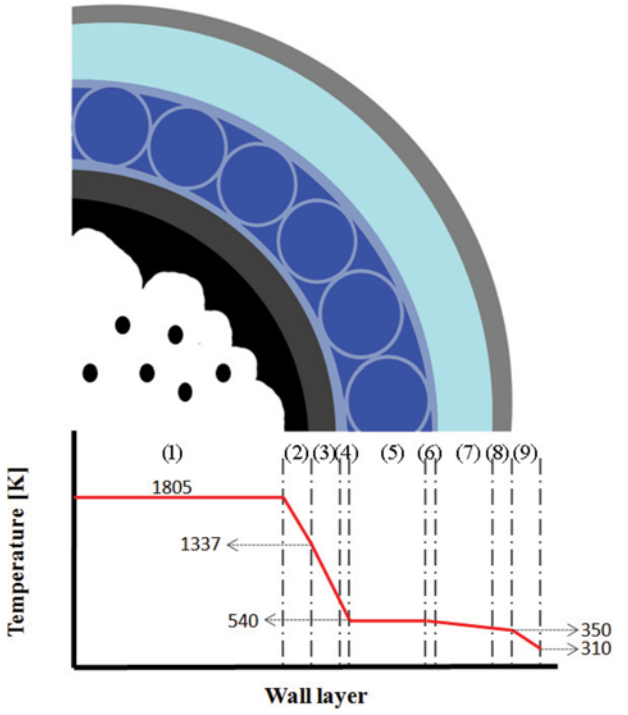

Fig. 6. Temperature profile along the gasifier wall at heights of 4-10 m.

(1) Gas
(2) Slag
(3) Refractory
(4) Membrane$_{in}$
(5) Water
(6) Membrane$_{out}$
(7) Air
(8) Steel
(9) Ambient

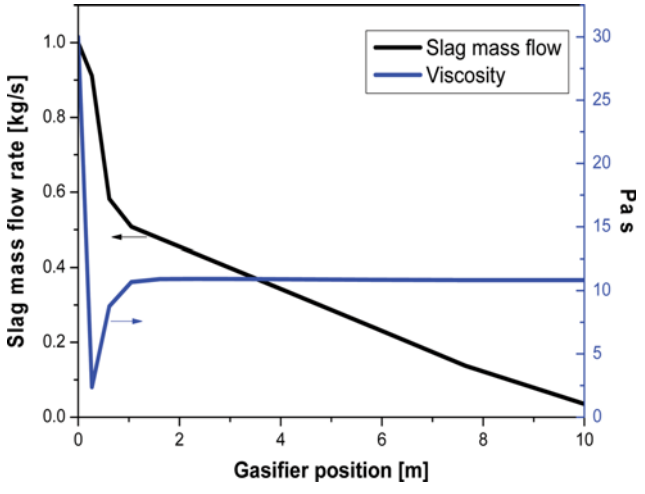

Fig. 7. Slag viscosity and mass flow rate profiles.

7. The mass flow is due mainly to slagging on the gasifier wall. The slag viscosity and mass flow rate depend on the region in the gasifier, because the slag formation process has a greater influence in certain regions. The mass flow increases gradually from the top of the gasifier to its end. This information can be used to determine where a thick slag layer would form easily. Viscosity directly affects the slagging process. Near the entrance of the gasifier, vis-

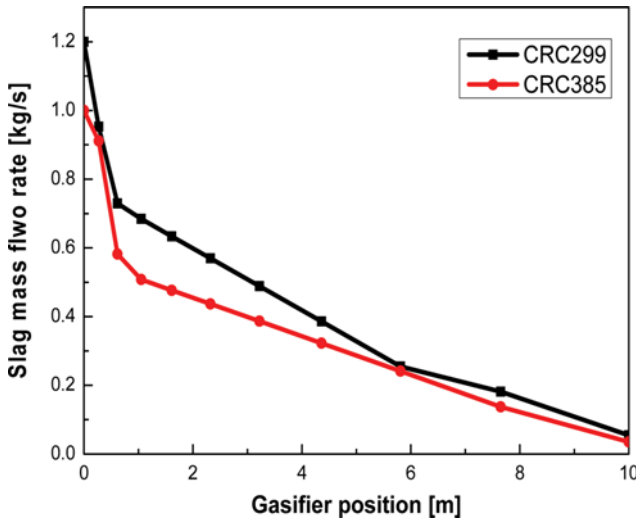

Fig. 8. Slag mass flow rates for two types of coal.

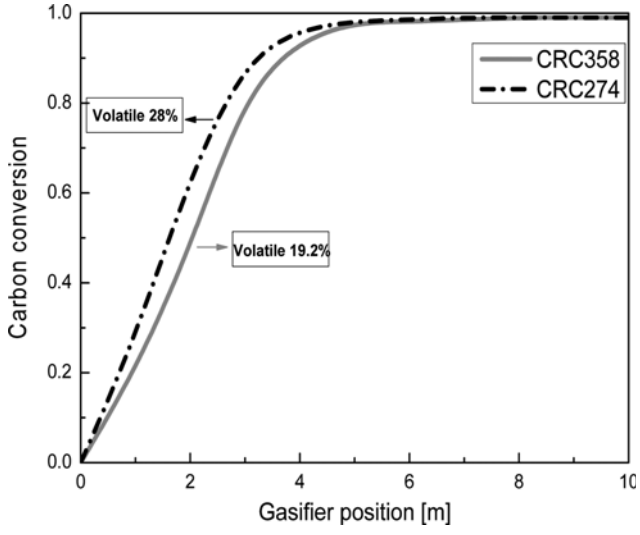

Fig. 9. Carbon conversion along the gasifier length for two types of coal.

cosity decreases because of the rapid temperature increase. Low viscosity causes a rapid increase in mass flow. Several factors can affect viscosity, but from our results, we conclude that temperature is the main factor affecting viscosity in this system.

The slag mass flow rates for two types of coal are shown in Fig. 8. The rates show the same general trends for both the types. Under the same operating conditions, high-ash coal shows greater mass flow. The simulation results are consistent with data acquired from the actual process, and in both cases, temperature has a direct effect on the slag mass flow rate.

4. Carbon Conversion

Fig. 9 shows the carbon conversion ratios along the gasifier length. The use of coal with higher volatile content and less fixed carbon can greatly improve the gasification conditions. Because of the rapid liberation of volatiles, complete carbon conversion can be achieved. On the other hand, the combustion of volatiles results in the generation of large amounts of heat to promote gasification. Accord-

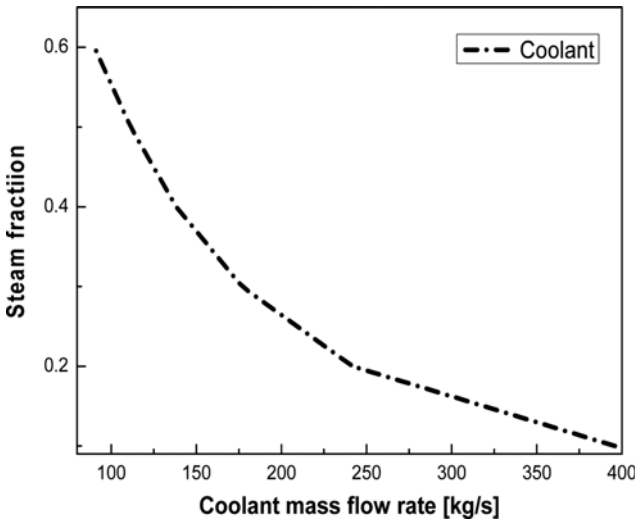

Fig. 10. Effect of coolant mass flow rate on steam fraction.

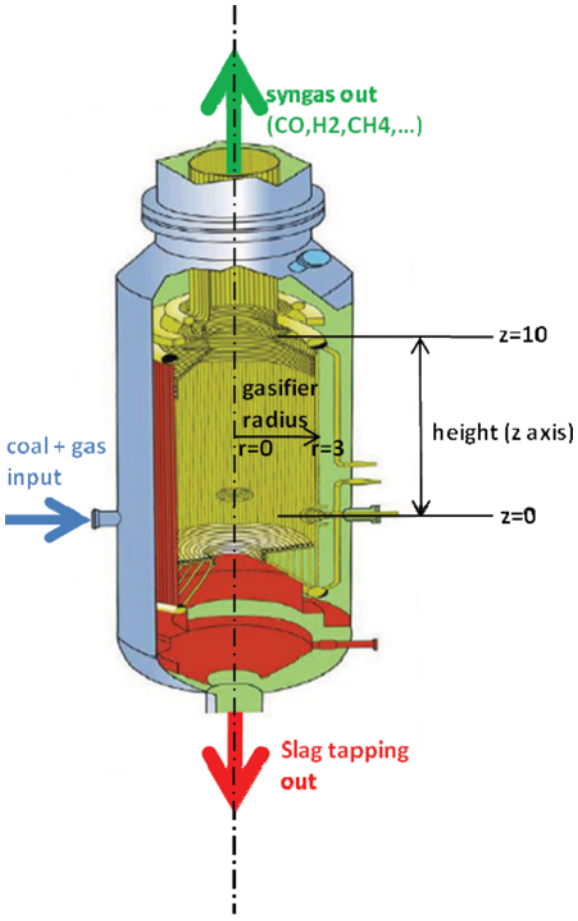

Fig. 11. Schematic diagram of Shell gasifier.

ing to the simulation results, complete carbon conversion is almost highest at the front of the gasifier. This seems to be a common feature of most commercial entrained-flow gasifiers.

5. Coolant Steam Fraction

Fig. 10 shows the effects of the coolant mass flow rate on the steam

fraction. As mentioned in the discussion of the temperature profile along the gasifier wall, no obvious temperature increase occurs within the water wall despite the transfer of heat from inside the gasifier, because this heat is used up for changing the state of the coolant. According to the simulation results, increasing the mass flow of the coolant can reduce the steam fraction, which is consistent with the design requirements. Therefore, a smaller coolant mass flow will reduce the cooling effect, and a large coolant mass flow can make the outlet steam fraction too low and will reduce the temperature in the gasifier.

CONCLUSIONS

A mathematical model was developed for simulating the performance of the Shell entrained-flow gasifier. This model can be used to determine the effects of the gasifier structure and size on its performance, and it includes a description of the kinetics of every major chemical reaction occurring in the gasifier. Thus, the model reflects real responses of materials in the furnace gasification process to different factors over time and models the actual process more closely.

The overall developed model was further refined into submodels. A model for the mass flow of the slag layer was constructed, and the influence of viscosity and the type of coal on the slag layer behavior could be modeled using it. Viscosity is a factor directly affecting the slag mass flow rate, and because high-temperature regions have the lowest viscosity, temperature also indirectly affects the slagging process. The steam fraction of the water wall is inversely proportional to the coolant mass flow. In addition to the operating conditions, the model calculates the influence of the type of coal on the gasifier performance parameters. Coal with a high volatile content helps to efficiently improve the conversion rate, whereas coal with a high ash-carbon content can increase the slag mass flow at the gasifier wall.

NOMENCLATURE

A : area [m^2]
C : gas concentration [$kmol/m^3$]
Cp : specific heat capacity [kJ/kg/K]
D : diffusivity [m^2/s]
f : friction factor
F : viscous frictional force per unit volume [N/m^3]
h : enthalpy (kJ/kg) or heat transfer coefficient [$kW/m^2/K$]
k : conductivity [kW/m/K]
km : bulk-to-wall mass transfer coefficient [s^{-1}]
K : equilibrium constant or absorption coefficient [m^{-1}]
mw : mole weight [kg/kmol]
m : mass flow rate [kg/s]
Nu : Nusselt number
P : pressure [atm, MPa, or Pa]
Pr : Prandtl number
Q : heat transfer rate per unit axial length [kW/m]
r : radius [m]
R : rate of chemical reaction [$kg/m^3/s$]
Re : Reynolds number
S : swirl number
t : time
T : temperature [K]
u : velocity [m/s]
X : mass fraction [kg/kg]
Y : yield [kg/kg]
φ : mechanism factor
δ : thickness [m]
ε : volume fraction [m^3/m^3]
μ : dynamic viscosity [Pa s]
ρ : density [kg/m^3]

Subscripts

af : ash free
cond : conduction
conv : convection
cs : cross section
dev : devolatilization
g : gas phase
hom : homogeneous reaction
het : heterogeneous reaction
i : gas-phase species
l : wall layer
rad : radiation
s : solid phase

REFERENCES

1. H. K. Seo, S. Park, J. Lee, M. Kim, S. W. Chung, J. H. Chung and K. Kim, *Korean J. Chem. Eng.*, **28**, 1851 (2011).
2. J. C. Corman, *Appl. Energy*, **10**, 243 (1982).
3. J. M. Beer, *Prog. Energy Combust. Sci.*, **26**, 301 (2000).
4. U. Buskies, *Appl. Therm. Eng.*, **16**, 959 (1996).
5. X. Chen, M. Y. He, I. Spitsberg, N. A. Fleck, J. W. Hutchinson and A. G. Evans, *Wear*, **256**, 735 (2004).
6. C. X. Chen, M. Horio and T. Kojima, *Chem. Eng. Sci.*, **55**, 3861 (2000).
7. C. X. Chen, M. Horio and T. Kojima, *Chem. Eng. Sci.*, **55**, 3875 (2000).
8. X. Z. Sha, Y. G. Chen, J. G. Cao, Y. M. Yang and D. Q. Ren, *Fuel*, **69**, 656 (1990).
9. R. Govind and J. Shah, *AIChE J.*, **79**, 30 (1984).
10. R. F. D. Monaghan and A. F. Ghoniem, *Fuel*, **91**, 61 (2012).
11. B. Sun, Y. W. Liu, X. Chen, Q. Zhou and M. Su, *Fuel Process. Technol.*, **92**, 1418 (2011).
12. D. Merrick, *Fuel*, **62**, 534 (1983).
13. W. P. Jones and R. P. Lindstedt, *Combust. Flame*, **73**, 233 (1988).
14. C. K. Westbrook and F. L. Dryer, *Combust. Sci. Technol.*, **27**, 31 (1981).
15. M. W. Chase, *NIST-JANAF Thermochemical Tables*, 4th Ed., National Institute of Standards and Technology, Gaithersburg, MD (1998).
16. C. Y. Wen and T. Z. Chaung, *Ind. Eng. Chem. Process. Des. Dev.*, **18**(4), 684 (1979).
17. B. H. Lee, S. I. Kim, S. M. Kim, D. H. Oh, S. Gupta and C. H. Jeon, *Korean J. Chem. Eng.*, **33**, 147 (2016).
18. G. N. Shannon, P. L. Rozelle, S. V. Pisupati and S. Sridhar, *Fuel Pro-*

cess. Technol., **89**, 1379 (2008).
19. F. Montagnaro and P. Salatino, *Combust. Flame*, **157**, 874 (2010).
20. G. Urbain, F. Cambier, M. Deletter and M. R. Anseau, *Trans. J. British Ceram. Soc.*, **80**, 139 (1981).
21. F. M. White, *Fluid mechanics*, 2nd Ed., McGraw-Hill, New York, NY (1986).
22. F. P. Incropera and D. P. DeWitt, *Fundamentals of heat and mass transfer*, 5th Ed., Wiley, New York, NY (2002).
23. L. D. Smoot and B. W. Brown, *Fuel*, **66**, 1249 (1987).
24. M. Gazzani, G. Manzolini, E. Macchi and A. F. Ghoniem, *Fuel*, **104**, 822 (2013).
25. J. D. De Graaf, *Shell coal gasification technology*, Lecture, Technische Universiteit Eindhoven (2011).
26. C. Higman and M. van der Burgt, *Gasification*, 2nd Ed., Elsevier Gulf Professional Publishing, Burlington, MA (2008). ISBN: 978-0-7506-8528-3.
27. D. Steiner and J. Taborek, *Heat Transfer Eng.*, **27**, 43 (1992).
28. Cooperative Research Centre for Coal in Sustainable Development (CCSD), Research Report 80 (December 2007).